Abstract of "A Program for Quantifying Humanlike Finger Forces Using an Anatomic Hand Tendon Model" by Richards C. Gilbert, Sc. M., Brown University, May 2001.

It is difficult for animators to manipulate the hands of animated characters to perform routine operations such as grasping objects and tool use. To create an automated grasping mechanism would be a great help for the animation community. One of the first steps in creating such a mechanism is to create a metric whereby we can measure the quality of a grasp based on the way an object is to be used. In this paper, we take one step closer to that goal by creating a tendon-based anatomical finger model that defines the continuum of forces that can be applied by a single finger. We evaluated this model by comparing our results with published experiments performed on human subjects and investigated how grasp forces vary with contact link, number of contacts, and finger joint angles. Our results confirm the utility of this model. It is hoped that this research will be expanded and continued until a full hand model and grasp quality measure are created.

Abstract of "A Program for Quantifying Humanlike Finger Forces Using an Anatomic Hand Tendon Model" by Richards C. Gilbert, Sc. M., Brown University, May 2001.

It is difficult for animators to manipulate the hands of animated characters to perform routine operations such as grasping objects and tool use. To create an automated grasping mechanism would be a great help for the animation community. One of the first steps in creating such a mechanism is to create a metric whereby we can measure the quality of a grasp based on the way an object is to be used. In this paper, we take one step closer to that goal by creating a tendon-based anatomical finger model that defines the continuum of forces that can be applied by a single finger. We evaluated this model by comparing our results with published experiments performed on human subjects and investigated how grasp forces vary with contact link, number of contacts, and finger joint angles. Our results confirm the utility of this model. It is hoped that this research will be expanded and continued until a full hand model and grasp quality measure are created.

A Program for Quantifying Humanlike Finger Forces Using an Anatomic Hand Tendon Model

by
Richards C. Gilbert
B. S., State University of New York at Stony Brook, 1999

A thesis submitted in partial fulfillment of the
requirements for the Degree of Master of Science
in the Department of Computer Science at Brown University

Providence, Rhode Island
May 2001

A Program for Quantifying Humanlike Finger Forces Using an Anatomic Hand Tendon Model

by
Richards C. Gilbert
B. S., State University of New York at Stony Brook, 1999

A thesis submitted in partial fulfillment of the
requirements for the Degree of Master of Science
in the Department of Computer Science at Brown University

Providence, Rhode Island
May 2001

AUTHORIZATION TO LEND AND REPRODUCE THE THESIS

As the sole author of this thesis, I authorize Brown University to lend it to other institutions or individuals for the purpose of scholarly research.

Date _____ _____

author's signature

I further authorize Brown University to reproduce this thesis by photocopying or other means, in total or in part, at the request of other institutions or individuals for the purpose of scholarly research.

Date _____ _____

author's signature

AUTHORIZATION TO LEND AND REPRODUCE THE THESIS

As the sole author of this thesis, I authorize Brown University to lend it to other institutions or individuals for the purpose of scholarly research.

Date _____ _____

author's signature

I further authorize Brown University to reproduce this thesis by photocopying or other means, in total or in part, at the request of other institutions or individuals for the purpose of scholarly research.

Date _____ _____

author's signature

This thesis by Richards C. Gilbert is accepted in its present form by
the Department of Computer Science as satisfying the thesis requirement
for the degree of Master of Science.

Date _____ _____

Nancy Pollard, Director

Approved by the Graduate Council

Date _____ _____

Peder J. Estrup, PhD.
Dean of the Graduate School and Research

This thesis by Richards C. Gilbert is accepted in its present form by
the Department of Computer Science as satisfying the thesis requirement
for the degree of Master of Science.

Date _____ _____

Nancy Pollard, Director

Approved by the Graduate Council

Date _____ _____

Peder J. Estrup, PhD.
Dean of the Graduate School and Research

Acknowledgements

I would like to give all the glory to Jesus Christ. Any success that I might have is completely because of His work in my life. Before giving my life to Him, I was a miserable creature, and I did not even know it. He has guided me through an awesome life of adventure and wonder. I owe Him absolutely EVERYTHING I have. If you do not know Jesus personally and can not say for sure that if you die today you will be going to Heaven, then I know that you have a huge hole in your heart that only He can fill. All you need to do is ask.

After Jesus, I'd like to thank my awesome family for many, many nights spent away from them in the toils of academia. My wife, Bärbel, has supported me and encouraged me in every endeavor. She truly is to be praised. Without her, I would never have made it to this place, and it is a very good place indeed. Thank you very much, my love!

A huge thank you goes to my children, Jamie and Camelot, who patiently waited many nights at the dinner table for me while I was finishing up some code. They have been patient and loving as I have worked my way through school. You two have brought so much joy in my life.

And a thank you should go to my mother, who always loved to hear what I was up to. She is always encouraging, always supportive, and always laughs at my jokes!

The greatest thanks has to go to Jesus. Thank you Jesus for *EVERYTHING*!!!

Contents

List of Figures

Chapter 1

Introduction

Enabling animated characters and robots to grasp various objects is a difficult task. Currently, it requires painstaking artist manipulation of 3D hand models to move into a grasping pose around an object. Typically, it is avoided.

If this process of creating feasible grasps could be automated, it would offer the animation world a new tool which would bring more realism to character animation. Additionally, the implications in robotics make this problem one of substantial significance.

The first step in creating an automated grasping mechanism is to create some sort of automatic grasp quality measure. Once we find a how good a particular grasp is, we can then compare among a number of grasps and choose one that is the best. This would be even more compelling if the grasp quality were not simply discrete, but existed on a continuum. A continuum of quality measures would give us the ability to start from a rough guess of a quality grasp and perform a search over the continuum to optimize the grasp.

One way of measuring grasp quality is by comparing forces that can be applied to an object (along the above continuum) to forces required to complete the task, or use a tool. An intuitive example would be something like a hand planer. Such a tool has a definite set of forces that must be applied to the object to complete the task.

We know a great deal about hand anatomy and its ability to produce various forces. Specifically, in this project, we will use this knowledge to build and evaluate a model of the forces that can be applied to an object by the index finger when it is in different configurations. If the results generated by this model seem promising, the model could be extended to include the entire hand. If we then placed the fingers in a grasping configuration, using knowledge of the task requirements (i.e. required forces to be applied on the object), we could compute a quality measure. [**?**]

More specifically, in this paper, we propose a tendon-based finger model that will serve as the basis for creating a grasp quality measure as described above in the future. The model tries to duplicate the tendon locations and maximal forces along those tendons as observed in human cadavers [**?**]. It then calculates the range of possible joint torques that can be produced around each joint in the finger. From there, it finds the force created at the contact point(s), and finally the aggregate force

generated at the object's center of mass.

The experiments that we ran for this paper are divided into two distinct categories: Simple Model Verification and Generated Force Variation.

1.1 Simple Model Verification

To verify the validity of our model, we duplicated some human experiments that were done by Valero-Cuevas et al. [**?**]. In their experiments, subjects placed their index finger in a receptacle that could measure maximum force generated in each of five distinct directions.

The maximum forces were measured via a pressure plate that was placed orthogonal to the force generated. Friction was reduced so as to localize the forces as closely as possible to the axes.

The human experiments were well documented, and we were able to duplicate the conditions of the experiments within our model. A major difference between the human trials and ours is that we are measuring the theoretical maximal forces that can be created by the index finger. The results from the human trials record only the mean maximal forces over the subject population that could be comfortably exerted by the human subjects. We therefore expect our results to be significantly higher than those from the human trials.

The results of this initial model verification were quite promising. Most of the directions measured generated forces that were two to three times the mean maximal forces found by Valero-Cuevas et al. This lends credibility to our finger model that we do have at least an approximation of the theoretical maximal forces that can be generated by a human finger.

Two exceptions to the above multiplication factor of two or three were found when moving the finger side-to-side (in the medial and lateral directions). We found that our model produced maximal forces that were close to the experimental means found in the human models. In viewing the variations of forces that can be produced by the finger, we did not look much at these directions, so for our purposes, the forces that our model generated are sufficient. However, this is one area that could use more work in the future.

1.2 Generated Force Variation

After verifying that our model was at least close to what should be expected with a maximal force model, we turned our attention to studying some variations of the hand configuration and contact point positions. The goal of this set of experiments was to examine the various force plots that can be generated by the finger model. Initially, we verify that the finger model does indeed create a wide range of possible forces. Then we try to determine what factors combine to create the variations. The result of these experiments were promising, and more work should be done in the future to expand this model to include the entire hand.

The experiments that are described below were based on photographs of a hand holding either a ball or a small travel clock. They are chosen to give us a sampling of the range of possible finger

configurations, and they are by no means meant to represent a complete range of configuration possibilities.

1.2.1 Various Hand Configurations

We begin the study with a single contact point finger configuration identical to the configuration in figure 1.1. The index finger is in a "relaxed" positioning, holding a ball. We use this initial finger configuration as a basis for interpreting the other configurations.

From figure 1.3, the reader can get a better idea of how the model works. Forces acting on the tendons in the finger create torques about each of the joints. These torques then in turn create forces acting on the object at the contact point(s). The total combination (as found in a convex hull) of all the forces is clipped to friction limits and used to calculate the total forces that can be applied to the object at the Center of Mass.

The next configuration is with the finger almost fully extended. We keep the one contact point on the third pad (farthest out from the hand). This is to see what differences and/or similarities there are between this configuration and the above one.

The ball is then moved closer to the hand so that the contact point is on the second pad of the finger. This configuration generated the most downward force of all the single contact point configurations. This was an encouraging result as it helped to verify the effects of reducing the moment arm on force generation in the finger.

The travel clock is then used for the next three experiments. The first is nearly identical to the first experiment of the ball. However, there are subtle differences in the hand configuration that give some variation in the maximal force plots. This gives us some good insight into what attributes contribute to create different force possibilities.

We then clamp the travel clock in between the finger with contact points at the first and the third finger pads. This shows us the effect that adding the symmetric contact points has on the force plots.

In an attempt to isolate the effects of each contact point, we then use the exact configuration as the preceding experiment and completely ignore the contact point on the first pad (closest to the hand).

The experiments that we ran tended to produce possible force plots that are both feasible and varied. We were pleased with the results of the experiments, and we conclude that this model is one that should be expanded and improved.

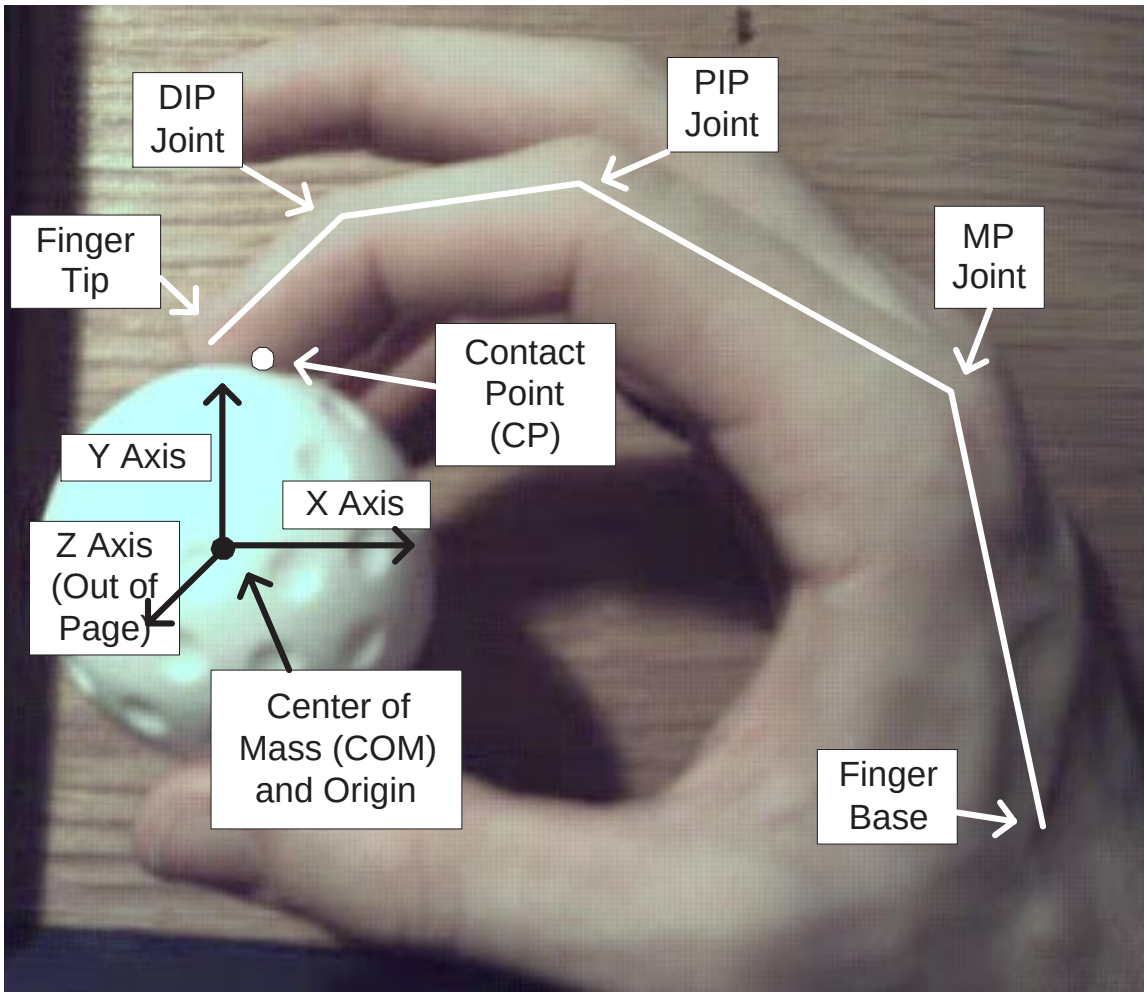

Figure 1.1: Diagram of bone structure for a typical experiment including axes.

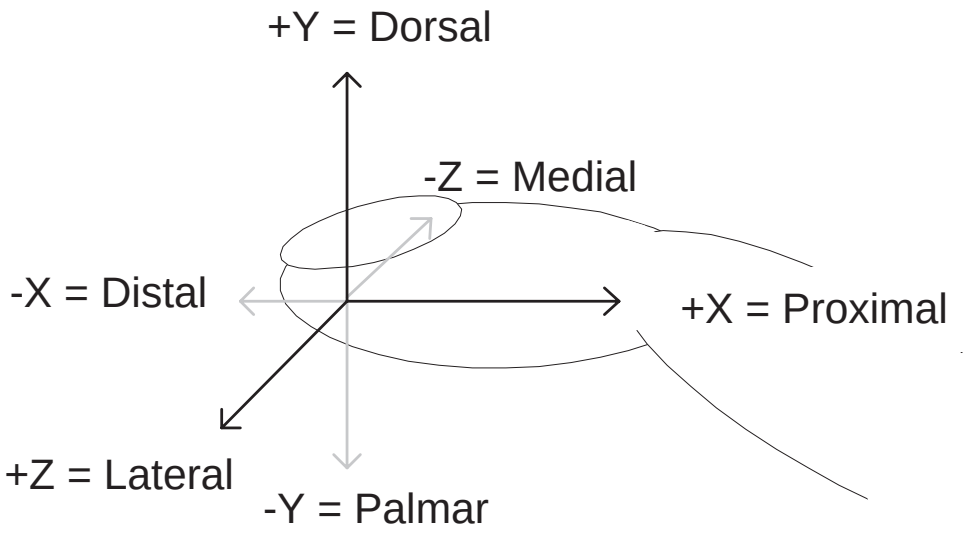

Valero-Cuevas:	Palmar	Dorsal	Distal	Proximal	Medial	Lateral
Our System:	-Y	+Y	-X	+X	-Z	+Z

Figure 1.2: The coordinate system used in the Valero-Cuevas human trials. The coordinate system is oriented in the center of the finger tip. That is, the coordinate system is based in the distal link's frame of reference.

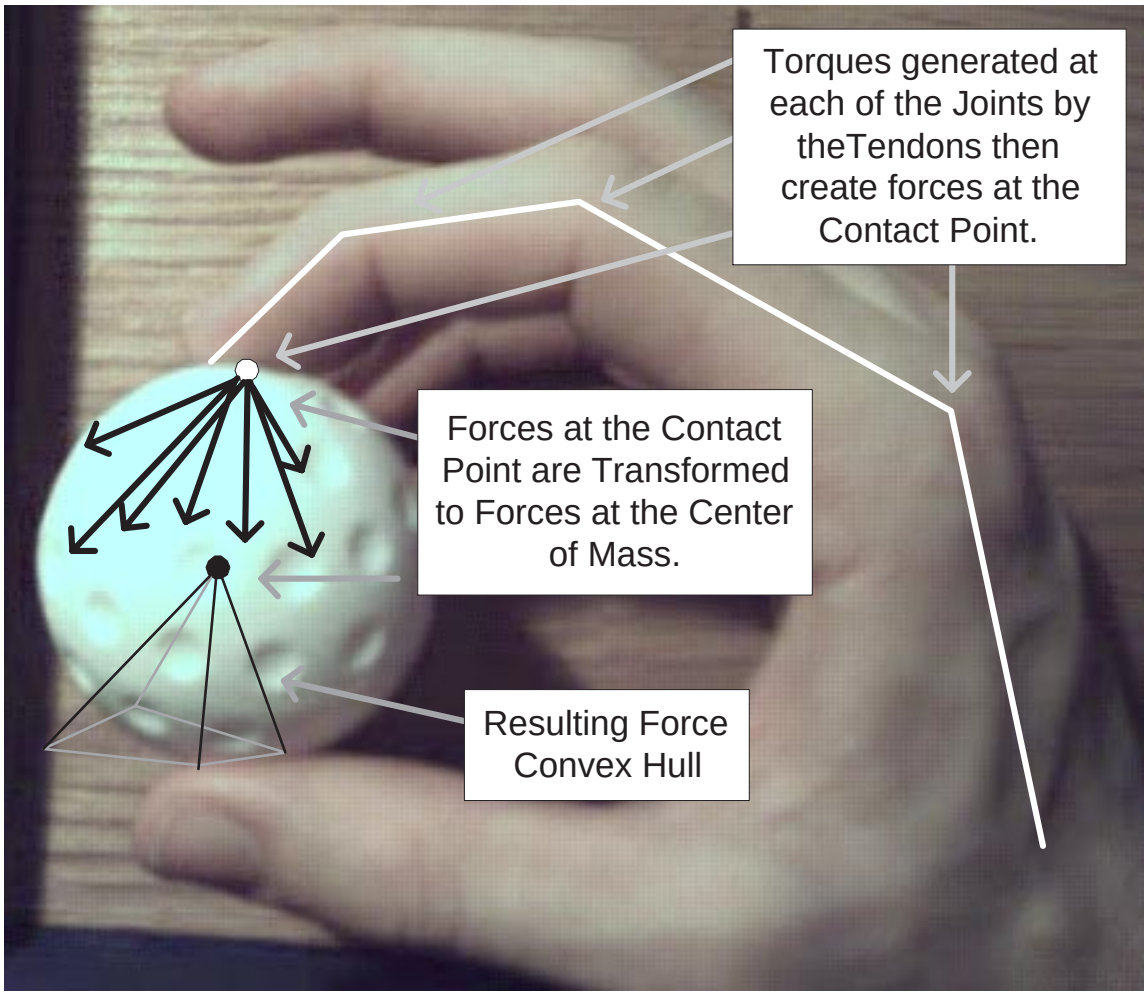

Figure 1.3: Brief explanation of the finger model. The tendons in the index finger create torque around each of the joints. These torques then create forces acting on the object at the contact point. Those forces are clipped to friction limits and transformed to represent the aggregate possible forces that can be applied to the object at the center of mass.

Chapter 2

Technical Details

2.1 Details of the Program

The Program (fig. 2.1) works with one finger at a time. It is assumed that the finger is in contact with a single object. The contact may take place at more than one contact point, and the object may be positioned in any location around the finger. For any given finger configuration, each joint location must be specified as well as the contact point(s), center of mass, and the friction coefficient. After this information is pulled into the program, it begins the calculations. Based on the joint locations specified, the Program takes data obtained from human cadavers [**?**] and calculates the rest of the anatomical data that it needs.

As seen in figure 2.1, the first step is to generate the extreme muscle activation levels so the joint torque extremes can be computed. The force extremes at the contact point(s) can then be calculated from these torques at the joints.

The program then converts the forces to halfspace representation and adjusts the forces according to the friction constraints.

The result at the end is a 3D space (a convex hull) of all of the possible forces that can be generated on the object at the contact point(s). The surface of this hull represents the maximal forces that can be applied to the object in the given finger configuration.

2.2 The Finger Model

There are a many ways to model a finger with all of the tendon and joint information. In our finger model, shown in figure 2.3, the proximal coordinate [1] frames were fixed to the proximal bones and placed at the points of rotation. The distal coordinate frames were fixed to the distal bones and offset from the points of rotation. The tendons were modeled as existing in a rigid sheath that held

[1] Proximal simply refers to the direction towards the hand, and distal is in the direction away from the hand (out towards the tip of the finger). See figure 1.2.1 for more details on the coordinate system.

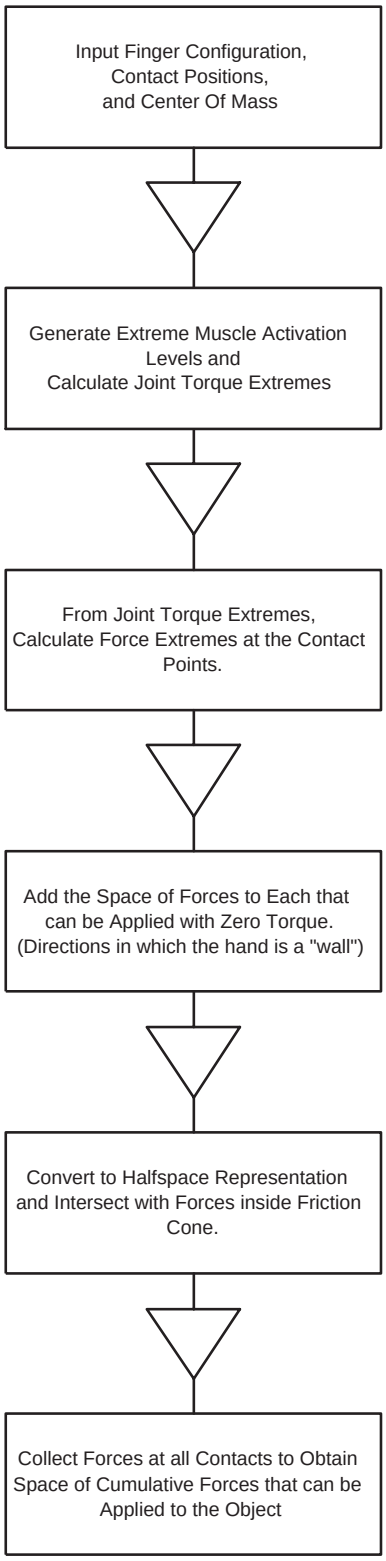

Figure 2.1: A flow chart representing the various stages that the program needs to go through.

Joint	Tendon Crossing Joint
DIP:	Terminal Extensor (TE)
	Flexor Profundus (FP)
	Fake1 (FAKE1)
	Fake2 (FAKE2)
PIP:	Extensor Slip (ES)
	Radial Band (RB)
	Ulnar Band (UB)
	Flexor Sublimis (FS)
	Fake1 (FAKE1)
	Fake2 (FAKE2)
MP:	Long Extensor (LE)
	Radial Interosseous (RI)
	Ulnar Interosseous (UI)
	Lumbrical (LU)

Figure 2.2: The tendons modeled with their short names and the joints that each tendon crosses.

them in a constant position relative to the proximal and distal bones. As seen in figure 2.3, the proximal end of the tendon sheath is fixed at point $R_{i,p}$ in the proximal frame, and the distal end of the sheath is placed at point $R_{i,d}$ in the distal frame. However, tendons were allowed to freely cross the joints outside of the sheathing. What is important for computing torque that the tendon can apply about a joint is the moment arm created by the tendon as it crosses the joint. Note that this moment arm varies with joint angle.

Measurements used to construct the model shown in figure 2.4 were taken from human cadaver specimens. For our model, the mean was taken from dimensionless data found in [**?**]. Dimensionless measurements were scaled to a particular individual based on the length of the central bone of the index finger (length O_2O_3 as shown figure 2.4).

Joint information was specified by marking a photograph with a finger in a particular pose (Such as found in figure 1.1). The poses varied according to experiment. The finger in the photograph included markings at the joint locations. These joint locations were then used to determine the joint angles and absolute locations of the tendons.

For our experiments, we analyzed planar grasps only, with all joint locations at Z=0.0. Therefore, the initial joint angles at each of the joints were limited to only be around the Z-axis. This was done for simplicity as we were attempting to verify the underlying model. By limiting initial joint positions to two dimensions, we eliminated the need to consider potential issues involving Euler angles. Despite this limitation, because the model allowed for tendon locations to be anywhere in three-dimensional space around the joint locations, ability to apply forces with this finger model was truly three-dimensional.

The other points specified in our model were the contact points and the object's center of mass (COM). Each contact point included a specification for which finger pad it was associated with. This was critical for accurately computing the hand Jacobian matrix (see below).

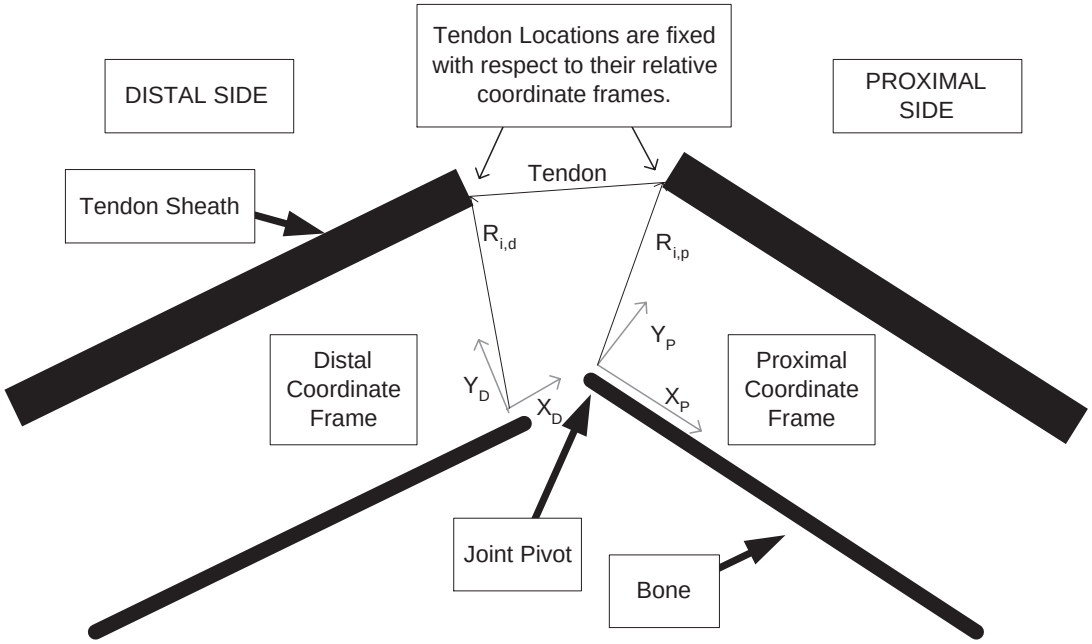

Figure 2.3: A diagram of the joint model used. The tendons travel through tendon sheaths that run parallel to the bones on either side of the joint. The proximal and distal tendon sheath openings are defined in relation to the proximal and distal coordinate systems (by $R_{i,p}$ and $R_{i,d}$) respectively). The relation remains fixed. That is, $R_{i,p}$ is constant in the proximal coordinate frame, and $R_{i,d}$ is constant in the distal coordinate frame. Notice that the moment arm from the joint changes with joint angle.

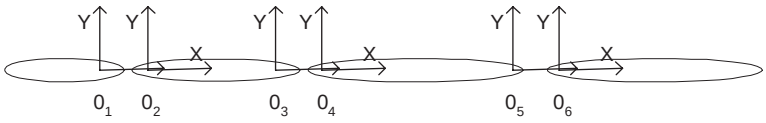

O_1O_2	O_2O_3	O_3O_4	O_4O_5	O_5O_6
0.22 +/- 0.4	1.0 +/- 0	0.29 +/- 0.04	1.94 +/- 0.28	0.45 +/- 0.05

Figure 2.4: Diagram of bone model showing distal (left) and proximal (right) coordinate systems.

All of the finger's motions and forces are linear with regards to muscle activation levels on the individual tendons. Therefore, when we have all of the points detailed above, the entirety of the finger mechanics can be modeled as a series of linear equations. This is exactly what we do.

One addition that was included in the finger model was the use of two extra tendons on the lateral and medial sides of the finger. (See figure 1.1 for details about positioning and coordinate systems). These imaginary tendons could generate equally large amounts of force at the DIP and PIP joints in opposing directions. The result of these two tendons was to mimic the effects of the ligaments in the joints. This was an attempt to guarantee stiffness in the DIP and PIP joints in the lateral and medial directions.

2.3 Math Details

Once the points of the finger were read in by the program as described above, the mean cadaver data was scaled to reflect the actual finger's dimensions. From this information, we can find the joint angles of the finger. The dimensionless tendon positioning information (Figure 2.3) was then translated into absolute positions around an arbitrary origin (usually the object's COM). Additionally, all of the necessary force vectors ($\overline{Fmax}_i$ in figure 2.5) were determined from this resulting hand configuration.

The goal of this project is to map muscle activation levels to maximum forces that can be applied on a particular object. To do this, we first need to find the torques, $\tau_{\mathbf{J}}$ that can be generated around the joints. Once we do that, we can use the current hand configuration to map the generated torques to forces acting on the object.

To find the torque generated around a particular joint, we map the muscle activation levels of the tendons that cross over that joint to torques about that joint. This is a linear mapping. If we assume a vector $\overline{a}$ holds the activation levels corresponding to our 10 tendons (12 including the 2 imaginary ones) in the forefinger, then we can compute the joint torques, $\tau_{\mathbf{J}}$, that are created by the given activation levels for a certain hand configuration, θ. We can do this by introducing a matrix M and calculating the linear equation:

$$\tau_{\mathbf{J}} = M(\theta)\overline{a}$$

M in the above equation is a matrix that maps the muscle activation levels to the joint torques. To calculate M, we introduce $\overline{R_{i,p}}$. As seen in figure 2.5, $\overline{R_{i,p}}$ is a vector from the joint to the proximal tendon location of tendon i. We also have $Fmax_i$ which is the maximum force scalar that the corresponding muscle controlling tendon i can produce. The scalar $Fmax_i$ is found by multiplying PCSA (Figure 2.6 as taken from [**?**]) by the maximal muscle stress of $35N/cm^2$ [**?**]. This force is applied in the direction $(\overline{R_{i,p}} - \overline{R_{i,d}})$, therefore we have an equation for the vector $\overline{Fmax}_i$:

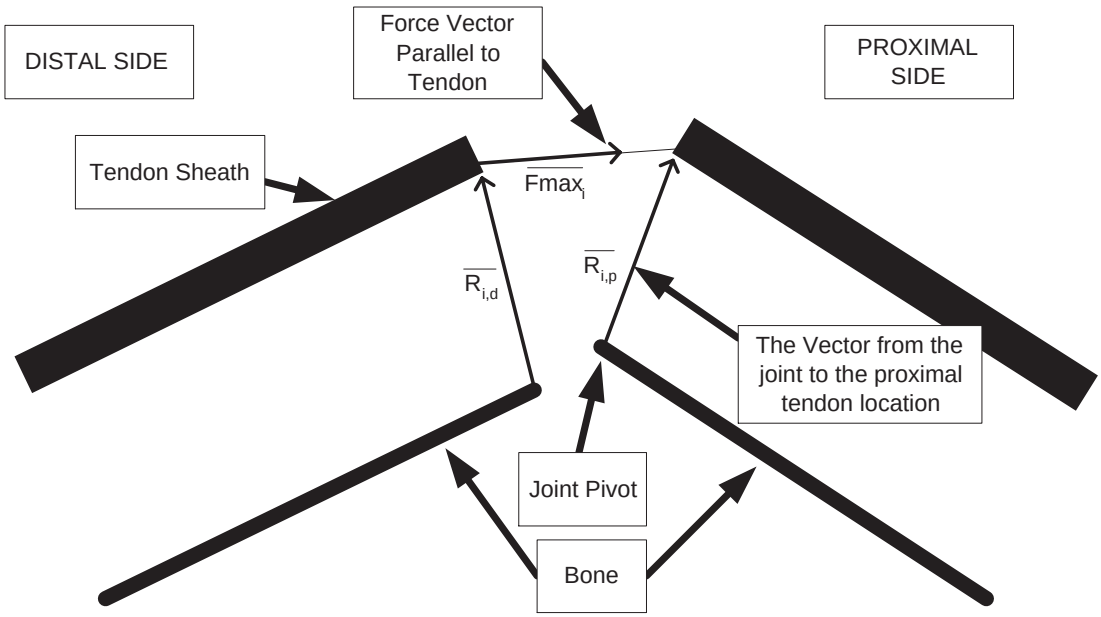

Figure 2.5: A diagram showing the relationship between the force vector and $\overline{R_{i,p}}$.

Tendon From Valero-Cuevas	PCSA	Tendon(s) in Our Model	Resulting Force
FDP	4.10	FP	143.5
FDS	3.65	FS	127.75
EIP	1.12	TE, ES, LE	87.85
EDC	1.39	TE, ES, LE	87.85
LUM	0.36	LU, RB	12.6
DI	4.16	RI	145.6
PI	1.60	UI, UB	56.0

Figure 2.6: PCSA values (from [**?**]) used and how we mapped them to our tendon model. Notice that EIP and EDC were added together and then mapped to TE, ES, and LE in our model. Also, LUM was mapped to LU and RB, and PI was mapped to UI and UB.

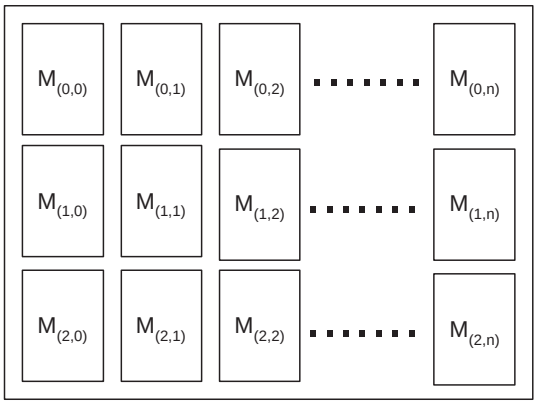

Figure 2.7: A diagram of the matrix M. Each sub matrix, $M_{(i,j)}$, that makes up the matrix M is a 3×1 matrix.

$$\overline{Fmax_i} = Fmax_i \frac{(\overline{R_{i,p}} - \overline{R_{i,d}}}{||(\overline{R_{i,p}} - \overline{R_{i,d}}||}$$

This results in the equation for any joint i and tendon j, $\overline{R_{j,p}}$ is the vector from joint i to the proximal tendon sheath opening of tendon j. So we have:

$$M_{(i,j)} = \overline{R_{j,p}} \times \overline{Fmax_j}$$

We set the range of muscle activation levels to between 0 and 1. By going through our procedure, we are looking for the space of valid torques that can be computed by feeding in the extreme points of the activation levels (as defined by a hypercube) through matrix M.

Each $M_{(i,j)}$ is a 3×1 matrix mapping activation of a single tendon j to torque about a single joint i (Figure 2.7). Therefore, if there are 3 joints and n tendons in a given finger, the corresponding M becomes a $9 \times n$ matrix that maps muscle activation levels to joint torques.

We could also find the joint torques, $\tau_{\mathbf{J}}$, if we knew the forces at the contact points. By multiplying the transpose of the hand Jacobian matrix, J^T, of a given hand configuration, θ by the forces, f, exerted at all contact points, we have:

$$\tau_{\mathbf{J}} = J^T(\theta) f$$

However, we actually want the reverse mapping. That is, we will calculate the joint torques, $\tau_{\mathbf{J}}$, and we wish to find the forces created at all of the contact points. Therefore, we invert the above equation to find f:

$$f = J^{+T}(\theta)\tau_{\mathbf{J}} + \sum_j \alpha_j v_j$$

$J^{+T}(\theta)$ in the above equation is the pseudo-inverse of the Jacobian matrix, and v_j are the basis vectors spanning the nullspace of J^T. The term α_j is any scalar (positive or negative) weighting the

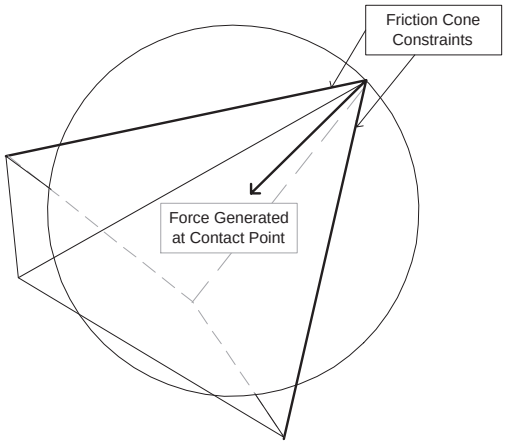

Figure 2.8: Friction cone constraints in 3D. The friction pyramid above is created on two orthogonal axes from the force direction. This will approximate the actual friction cone while still remaining linear.

basis vectors, v_i, that span the nullspace. In practice, we want to find a convex hull of legal applied forces. So we use the following sample points where α_j is a large scalar and $j = 1, 2, .., k$, and where k is the dimensionality of the nullspace of J^{+T}.

$$f_{j+} = J^{+T}\tau_J + \alpha v_j$$

$$f_{j-} = J^{+T}\tau_J - \alpha v_j$$

Friction between the finger pad and the object at the contact point(s) (Figure 2.8) is approximated by using the Coulomb friction model. The forces at the contact points are constrained within a friction cone that is centered at the inward-facing normal of the object's surface at the contact point. To maintain linearity within the system, the friction cone is approximated by a four-sided friction pyramid with the same characteristics.

The forces that result from the above equation are then intersected with the friction pyramid to create a convex hull of valid forces on the object at the contact point(s). This ensures that the forces that we ultimately generate are valid within a realistic model of friction.

Intuitively, as the coefficient of friction, μ increases (i.e. the surface is more "sticky"), the cone angle of the friction pyramid increases. As the friction between the finger and the object decreases, so does the cone angle of the pyramid. This reduces the extent of valid forces that can exist within the resulting friction pyramid.

The convex hull resulting from the intersection of achievable forces with forces lying within the friction pyramid then needs to be translated into a convex hull of valid forces applied to the object. This is another linear mapping that is accomplished by the use of a new matrix, G.

$$f_0 = Gf$$

The matrix G simply sums applied forces at the contact points and computes and sums the applied torque that would be generated about the object's center of mass due to these forces. The resulting vector f_0 represents the three-dimensional forces and three-dimensional torques that can be applied on the object when the finger contacts the object at the given contact points with the given friction constraints.

Therefore if we combine the above equations, we have a mapping from the 2^n combinations of n muscle activation levels, $\overline{a}$, to the convex hull of all possible force and torque values, f_0. Below are some examples. In the equations, $i = 1, 2, 3...2^n$, and a_i is the binary representation of i. Additionally, $j = 1, 2, 3...k$ where k is the dimensionality of the nullspace of J^{+T}:

$$f_{0,i,j+} = G(J^{+T}(\theta)M(\theta)a_i + \alpha v_j)$$

$$f_{0,i,j-} = G(J^{+T}(\theta)M(\theta)a_i - \alpha v_j)$$

$$f_{0,i} = G(J^{+T}(\theta)M(\theta)a_i)$$

From the above equations, for any one configuration of G, M, $J^{+T}(\theta)$, and n tendons, there are $(2^n + 2^{n+1} \cdot k)$ possible such resulting force vectors (k being the dimensionality of the nullspace of J^{T+}). Each possible v_j must be involved, and we use a negative as well as a positive alpha. A convex hull is then calculated for all of these $O(2^n)$ forces to find a three dimensional volume of possible forces on the object.

Once the above equations are computed, and we have our 3D convex hull, we can then look at the results to firstly determine whether or not the model is accurately modeling forces and torques that can be applied by the human finger. Secondly, once we have confirmed the validity of the model, we examine the results to gain insight into what factors of the hand configuration are the most and least influential in determining the maximal forces that can be applied to a particular object.

Chapter 3

Results

This section will be divided into two parts. Initially, we will discuss our efforts to confirm the validity of the finger model by duplicating experiments carried out on actual human subjects. The second section will then discuss experiments that we conducted by placing the finger model in various configurations that display some of the various force possibilities that can be created with our finger model. Included in this second part will be a discussion on the insight that we have gained as a result of these experiments.

3.1 Validity of the Model

In an attempt to verify the validity of this mathematical model of the human finger, we mimicked experiments carried out in 1998 by Valero-Cuevas et al [**?**]. In the experiments performed, human subjects placed the tip of their finger into a thimble-like receptacle and restrained their hand by grasping a vertical bar. They were then asked to exert the maximal force that they could in five orthogonal directions. Friction was minimal, within a friction cone of 16 degrees on either side of the force direction. Therefore, the results limited force to a well-defined direction. The maximum force that they could generate in each direction was then measured by the device, and the statistic mean was taken for all of the individuals.

This is exactly the experiment that we duplicated with our model. Within our model, we specified a hand configuration based on a human subject holding a vertical bar with the subject's figure slightly bent as it was in the Valero-Cuevas trials (figure 3.1). We used the muscle cross-section data that Valero-Cuevas et al. also used.

Since our tendons did not match up exactly with those tendons specified by [**?**], we combined the corresponding muscle data in a consistent way to map it to our tendon model. We did this by examining a graphical tendon model in the paper and matching the tendons with ours (Fig. 2.6).

For each of the five directions studied, we created an object at that location relative to the finger in our model. We used a consistent friction coefficient μ of 0.2867 to duplicate the 16 degree friction cone that was specified in the human trials.

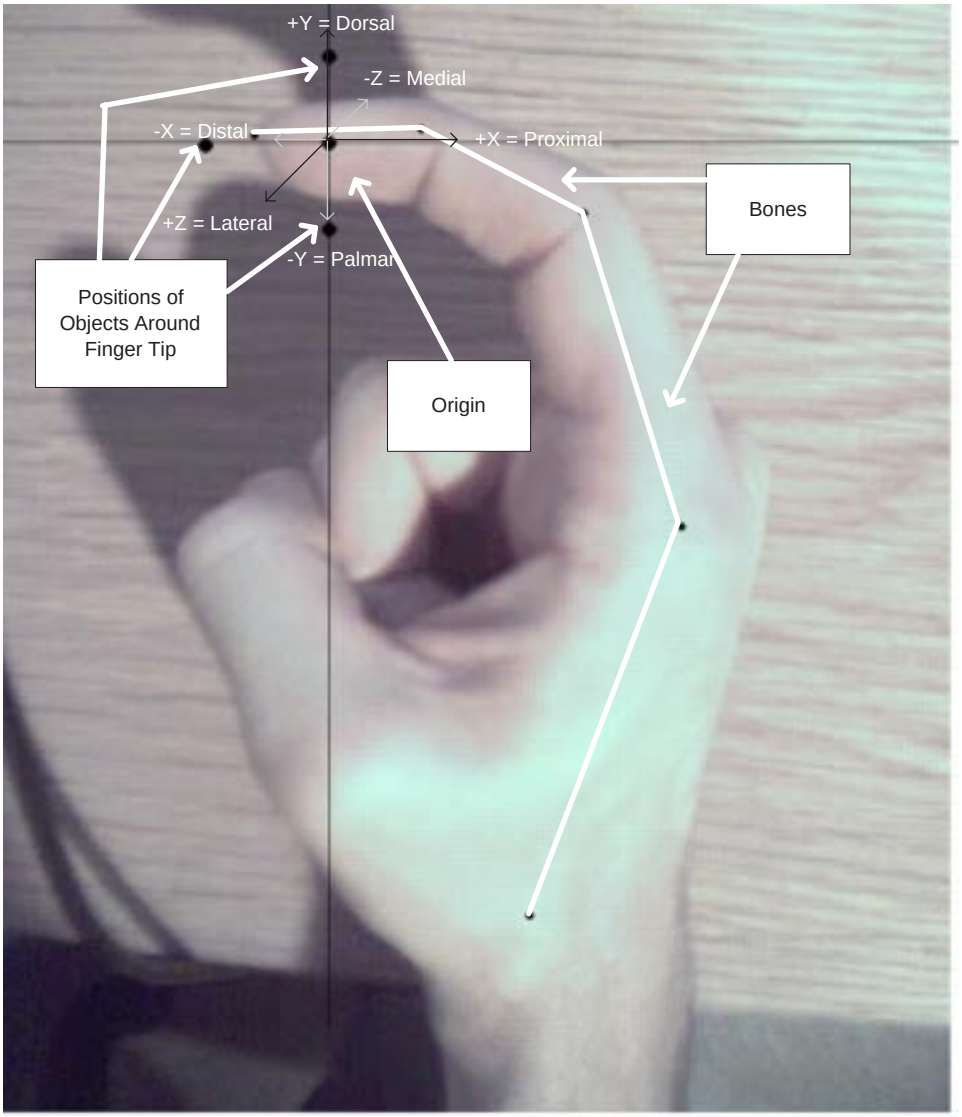

Figure 3.1: Photo of the hand configuration used to duplicate the human trials performed by Valero-Cuevas et al. Notice that in these experiments, the origin is moved to the center of the finger tip (inside it). Then small spherical objects are places around the finger tip to correspond to the axes emanating from the origin. The force that can be applied by the finger tip onto each of these objects in the appropriate direction is then noted and compared with the corresponding results of the human experiments.

Direction	Experimental Mean	Our Model Prediction	V/C Model Prediction
Palmar (-Y)	27.9 +/- 4.1	66.67	17.3
Dorsal (+Y)	7.5 +/- 1.5	14.90	4.1
Distal (-X)	24.3 +/- 8.3	75.16	17.4
Proximal (+X)	N/A	13.63	N/A
Lateral (+Z)	14.7 +/- 4.8	23.28	27.2
Medial (-Z)	22.9 +/- 7.8	18.86	15.0

Figure 3.2: Comparison of the results obtained by Valero-Cuevas et al. and those created by our finger model. Proximal is the opposite direction to Distal, and it was not recorded during the human trials.

The base of the finger was fixed at the start point, and the rest of the joints were assumed to be flexible. Finger joint positions had starting points at $Z = 0.0$, but from there were allowed to apply force in any (3D) direction.

Because our program is entirely deterministic, we only needed to run it once for each desired direction. We then took our result for each of the five orthogonal directions and compared it with the mean calculated among the human trials carried out.

We did run the experiment in the proximal direction (negative to the distal). This would simulate the receptacle being attached to the point of the finger, and the subject trying to pull his finger out. This was done for completeness as well as to give us insight into some of our other results.

It is critical to realize that our model deals exclusively with theoretical maxima based on average muscle cross sections and maximal muscle excitation. It is likely that humans are not able to control the muscles around the finger so exactly as to extract the maximal forces. When we compare them to the results from human experiments, then we should definitely find them to be well above the experimental mean. In fact, by nature of our using muscle excitation levels of 100%, there should be no human (or extremely few humans) with normal muscle size that could create the maximal forces.

Additionally, we completely eliminated any forces from the wrist. It is unclear what effects the wrist has on finger movement in the Valero-Cuevas trials. Therefore, what we are looking for are trends that give us an idea of how close this model is to the experimental results. If we can see that the generated forces in the five given directions are somewhat proportional to the experimental results, we can take that information into account while we are interpreting the results of various finger configurations. We deal with those in the next section.

As a reference to navigating through the following results, please refer to figure 3.1 for hand configuration.

One of the most significant results from these experiments for our purposes is that of the palmar forces created by the finger (Fig. 3.3). We notice from the table of results that our result of 66.67 N is just a bit more than double that of the human trial results of 27.9 N. This is a rather good result considering we are looking at a theoretical maximum. There could be a number of factors that prevent a human from obtaining this result.

From there, the next most significant number is the distal result (Fig. 3.4). Our model's results

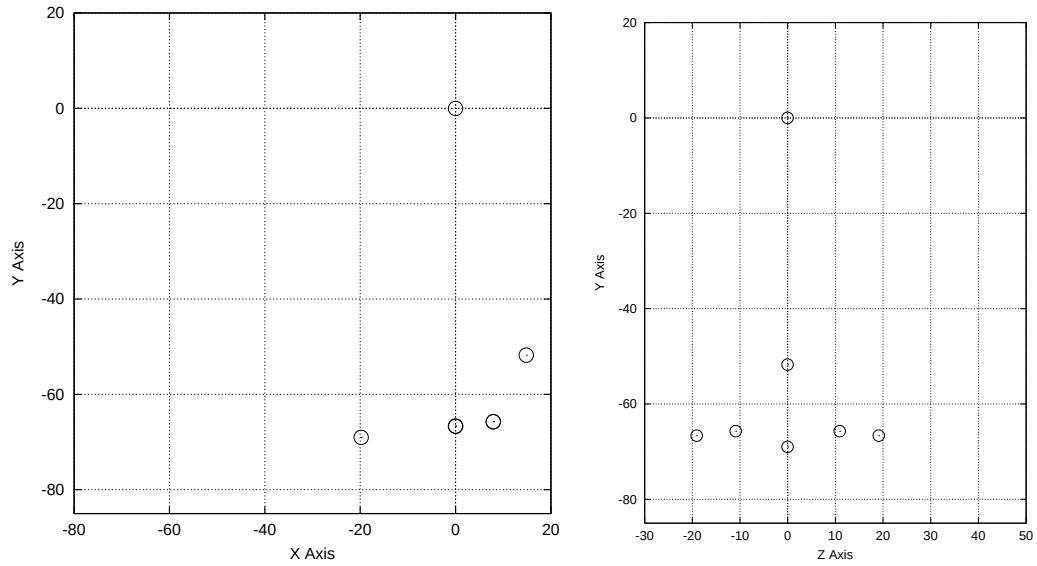

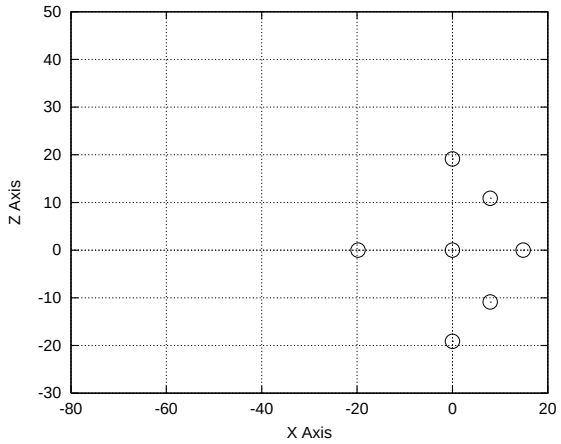

Figure 3.3: Palmar Forces (-Y) in the XY, ZY, and XZ Planes

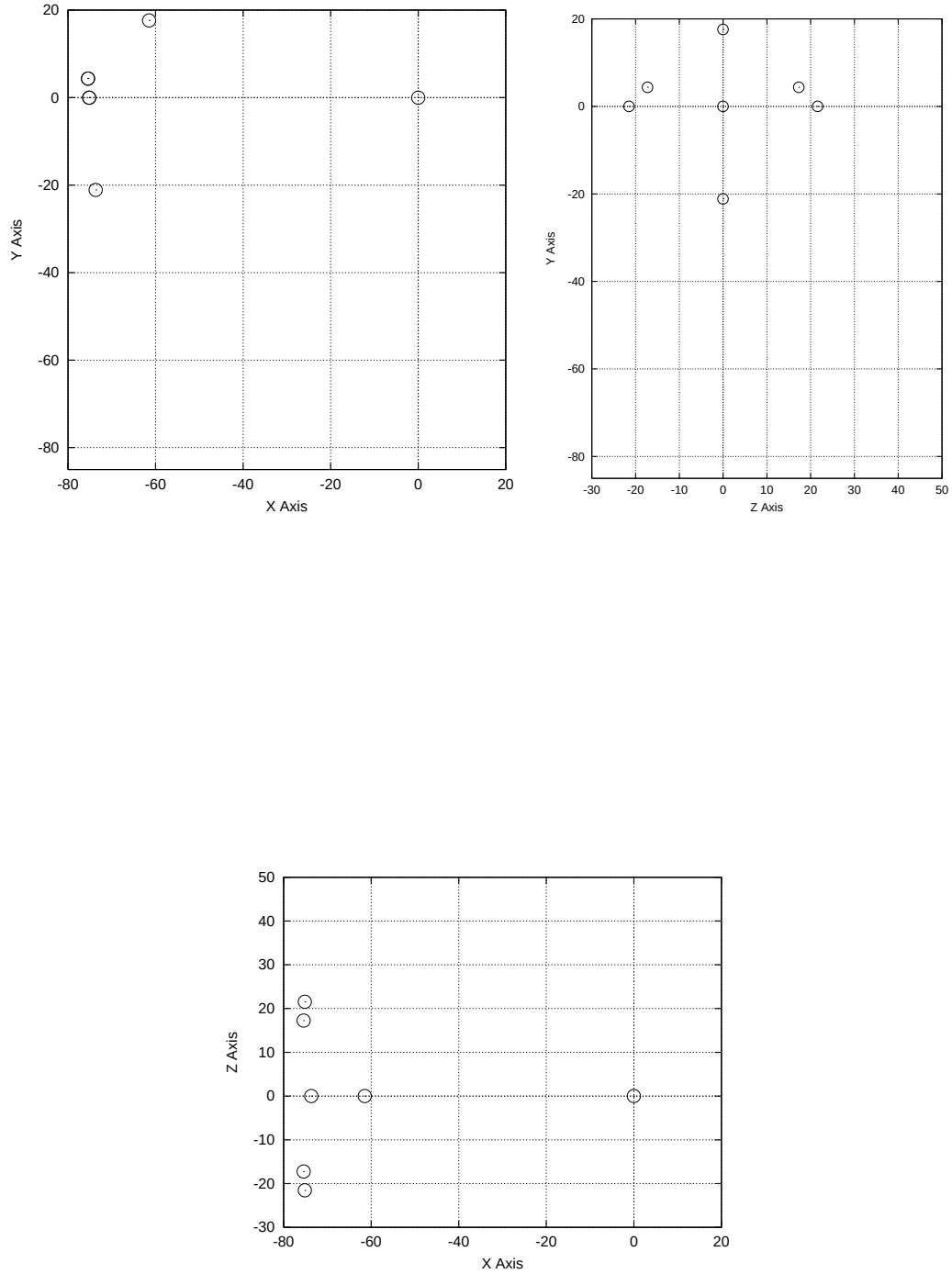

Figure 3.4: Distal Forces (-X) in the XY, ZY, and XZ Planes

(75.16 N) are almost three times that of the human trials (24.3 N). One detail to notice, however, is the fact that there was a wide range of forces in the human trials for the distal result. The standard deviation is 8.3. That is more than $\frac{1}{3}$ of the actual mean. If we take the outward reaches of the first standard deviation of the experimental results ($24.3 + 8.3 = 32.6$), then we come close again to a factor of two. However, even if we are looking at a factor of three, this result could fit in with a theoretical maximum for the distal forces.

The dorsal result (Fig. 3.5) essentially follows the pattern of the palmar forces in that there is a multiplication factor of almost exactly 2. Their experiments resulted in a mean of 7.5 N, with a standard deviation of 1.5. Our model gives a maximum of 14.90 N.

The lateral result of 23.28 N fits in well with the doubling factor found in the above trials. See figure 3.6 for a full plot of the lateral forces. While it is not quite double of the experimental mean of 14.7 N +/- 4.8, it is certainly significantly higher and approaching a factor of 2.

The last result that we included that parallels the human trials is the medial result (Fig. 3.7). Here, we are just below the mean or 22.9 N +/- 7.8, yet well within one standard deviation. Our model produced a result of only 18.86 N. The medial result was clearly the weakest in the group.

The above results reflect an attempt to correct the model in the medial and lateral directions by including two imaginary tendons running along the medial and lateral sides of the finger. These tendons were attached to muscles that could generate large amounts of force. The intuition was that these added tendons would play the part that the ligaments in the finger play to create a sort of constraint in the medial/lateral directions. When the forces on these muscles were one or two orders-of-magnitude above the forces produced on the other (actual) tendons, the lateral and medial results more than doubled to what they are above.

It is our belief that the model is somehow deficient in its accurate reproduction of forces in the medial and lateral directions. This does not affect our analysis later in this paper because we do not vary the location of the contact points along the Z-Axis (lateral/medial). Most of our analysis looks at the X-Y plane in determining validity of the various plots. There is some attention paid to the Z-Axis, but the analysis would not change significantly with increased force magnitude in the medial or lateral directions.

We included one last use of this model, and that is to calculate possible force generated in the proximal direction (Fig. 3.8). We note in the chart that the result of that was a maximal force of 13.63 N. This is about $\frac{1}{6}$ the maximal force generated in the distal direction. This explains why some of the experiments that we ran on different finger configurations seemed to have a stronger tendency towards the distal direction (-X).

The main conclusion that we can draw from our results here is that our finger model appears valid as a model of the maximum possible finger tip forces generated in the palmar, distal, and the dorsal directions. Without modification, we would not rely on the model to accurately predict medial or lateral forces. However, the bulk of the experiments that we have been working with primarily involve forces generated in all directions besides the medial and lateral. Our main emphasis in our experiments was in palmar and distal forces, and those were extremely close. Therefore, we

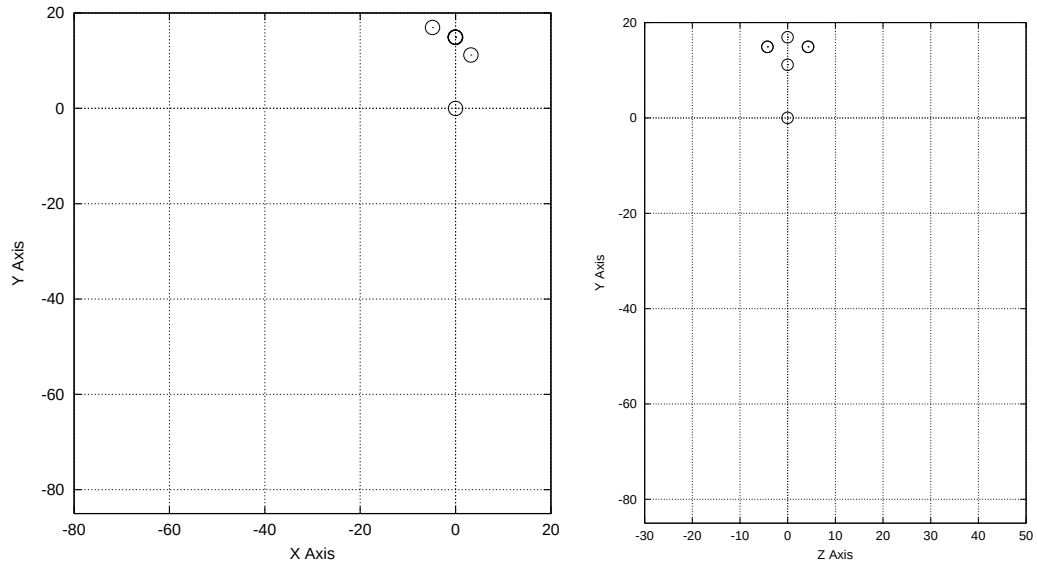

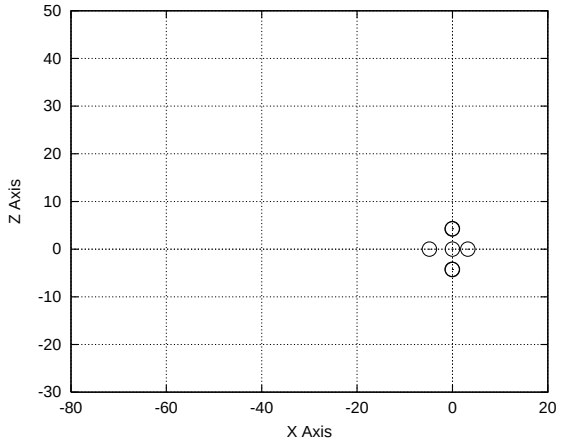

Figure 3.5: Dorsal Forces (+Y) in the XY, ZY, and XZ Planes

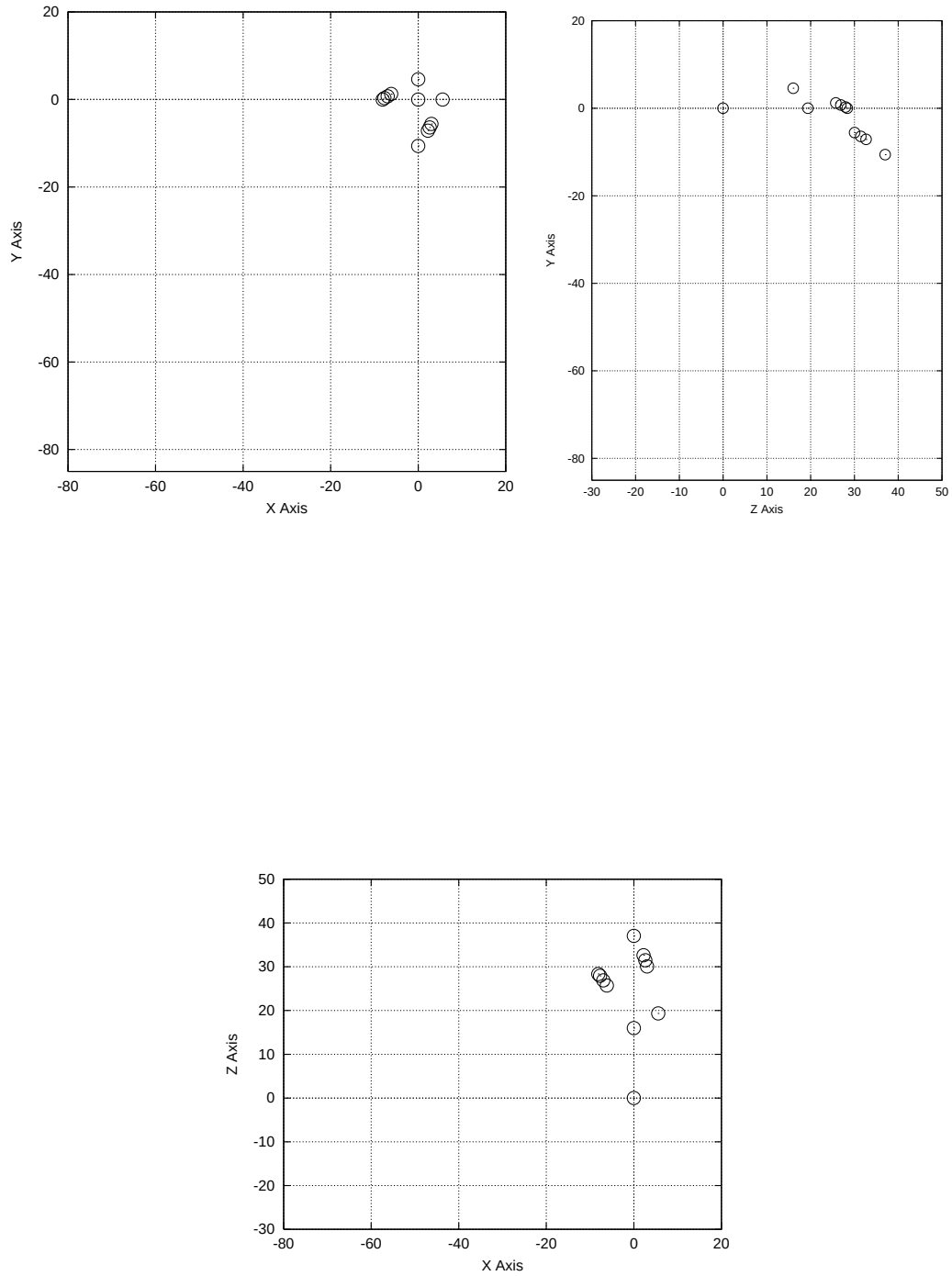

Figure 3.6: Lateral Forces (+Z) in the XY, ZY, and XZ Planes

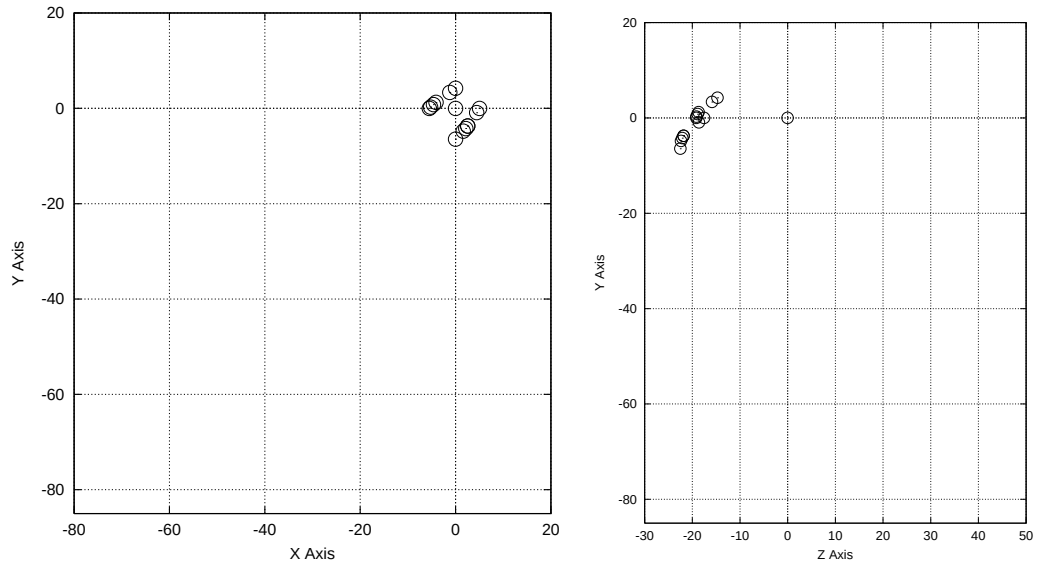

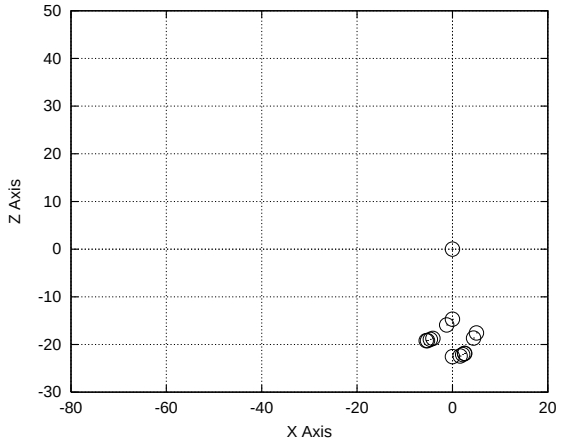

Figure 3.7: Medial Forces (-Z) in the XY, ZY, and XZ Planes

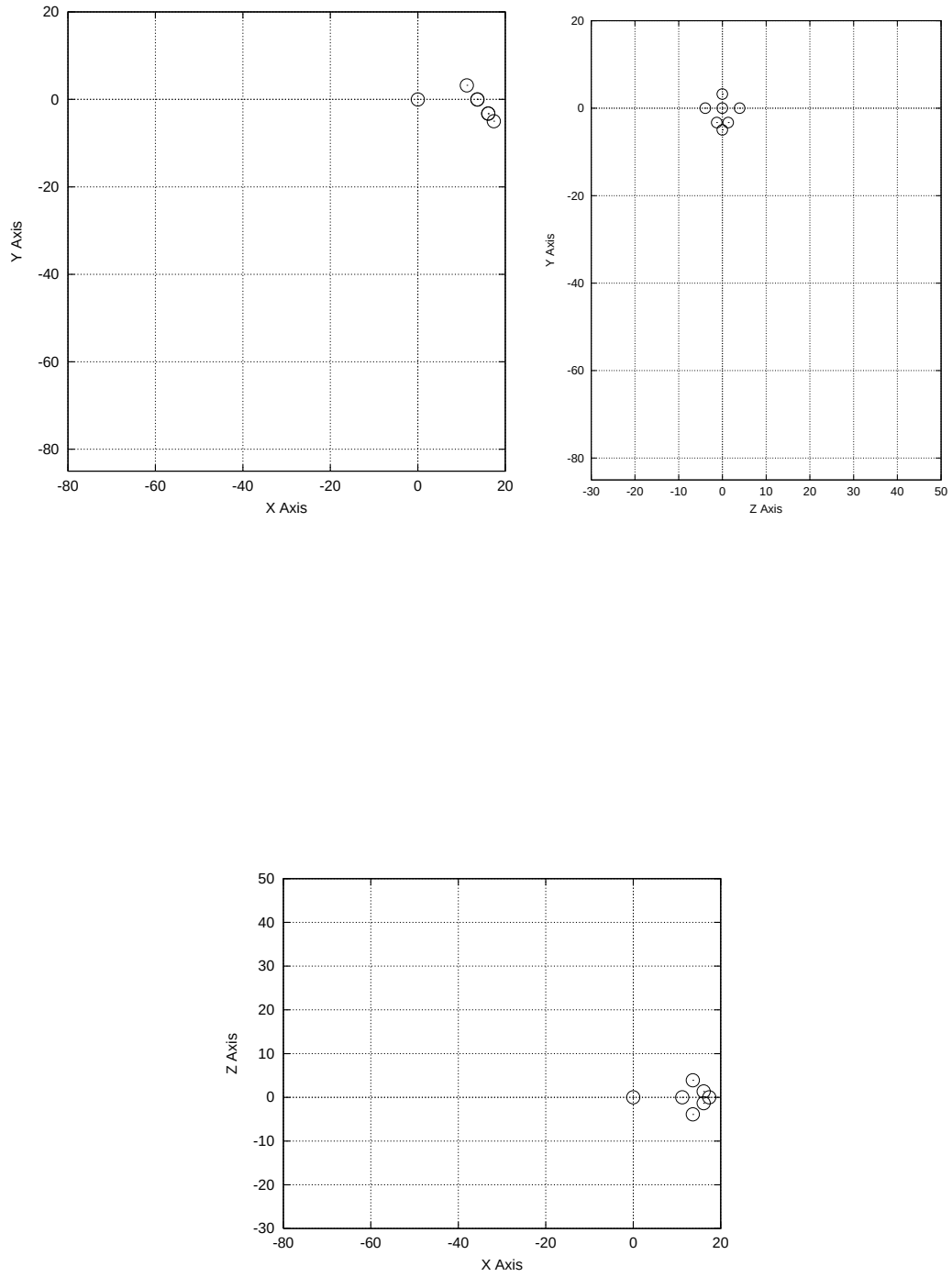

Figure 3.8: Proximal Forces (+X) in the XY, Y, and XZ Planes

conclude that, within the above constraints, the model is valid enough to give us some insights into the maximum forces that can be generated by the human finger for the goal of creating a grasp quality measure.

3.2 Variation due to Finger Configuration

Once we validated the finger model as outlined in the previous section, we then focused on viewing the results of various finger and object configurations. From these results, we could gain fresh insight into what factors affect the maximal force that can be applied to an object given a particular hand configuration.

In running these experiments, we sought to vary the number of contact points, the positions of the contact points, the associated finger pad that each contact point contacted, and the finger configuration in terms of initial joint angles and object-palm proximity. We did *not* vary the friction μ, nor did we vary the maximum muscle forces that could be generated. The friction is different than that specified in the human experiments, but it is constant over all the contrived hand configurations we are about to look at. For the purpose of the experiments, we were using the identical virtual finger grasping an object in varying ways.

Each of the plots are scaled identically in similar planes. That is, plots showing the XY plane for each finger configuration will have the same range and domain. This makes seeing detail of some of the plots more difficult, but it makes it easier to compare between plots of different hand configurations. This falls in with the point of these experiments, and that is to see what modifications to the initial configuration will change the magnitude and direction of the maximal forces that can be generated.

For each of the various finger configurations, we offer three plots of the forces involved. These plots are the XY, ZY, and XZ planes to show all three dimensions of force generation. For reference, a photo is included in each force plot figure. The photo represents the finger configuration as looking at the XY plane. The ZY plane would correspond to looking at the finger from its tip, and the XZ plane would be looking from the top.

3.2.1 One Contact Point on the Third Pad

The first finger configuration we will look at can be found in Figure 3.9. For identification, we will call the first finger configuration the "Natural" configuration only because we can use this as a reference point in studying the other finger configurations.

The first feature to notice in the force plots of the Natural configuration is that the palmar force (-Y) that can be applied is nearly equal to that of the palmar force result that was obtained in the last section. This is to be expected as the finger configuration in this example is nearly identical to that of the palmar experiment configuration.

We can notice that the angle of the friction pyramid has expanded significantly because the coefficient of friction (μ) was increased for these experiments from that of the Valero-Cuevas human

trials. This was so that the results would give us a simulation of a finger touching and manipulating real-world objects.

The force convex hull is skewed toward the distal (-X) direction. This can be seen in the XY and the XZ plots. Recall that when we duplicated the human trials from Valero-Cuevas et al., we added the theoretical value of proximal force (+X). We found this to be nearly $\frac{1}{6}$ that of the distal force that could be generated. This could certainly lead to the skewing of our results in the -X (distal) direction.

The -X skew certainly makes sense if one observes how much easier it is to push an object out in this type of grasp rather than pulling it into the palm. This skewing is seen throughout the rest of the results.

Otherwise, possible force in the +/- Z directions are relatively symmetrical. We can see the direct effect of the friction cone on the plot as it slopes out in the XZ plot.

We will compare the other results with this one.

3.2.2 Straight Finger With one Contact Point on Third Pad

The finger configuration found in figure 3.10 is similar to the Natural configuration in that it has one singular contact point on the third finger pad. It differs, however, in that the finger is stretched out and nearly flat.

The difference in the XY plot can be seen immediately. The finger is able to deliver more force on the object in the +/- X directions than the Natural configuration. We also see the -X skew mentioned earlier. However, now it is more pronounced.

Symmetry around the Z Axis remains, however, the finger is not able to generate as much force in the +/- Z directions as it could in the Natural configuration. This probably corresponds to the fact that the only medial/lateral forces that the finger can apply must happen around the MP joint. This is mainly due to the two fake tendons that were put in to mimic ligaments. This configuration lengthened the distance between the MP joint and the contact point, thereby increasing the moment arm. It could therefore not create as much medial or lateral force.

3.2.3 Straight Finger With one Contact Point on Second Pad

The finger configuration in figure 3.11 is clearly the most powerful configuration of those sampled. The XY forces stretch all the way to the limits of the graph. What does this tell us about the forces that can be generated by a finger? One possibility is that the DIP joint is acting as a limiting factor in the configuration of figure 3.10. Another possibility is that in bringing the center of mass (and the contact point) closer to the palm of the hand, we have decreased the moment arm to the MP joint. This could certainly increase the finger's ability to generate force at that contact point. The total increase is possibly a combination of both factors.

Unfortunately, we were unable to create a set of forces from a configuration having a single contact point on the first finger pad. If we had done so, we would expect to see that result be even

stronger than this one due to the PIP joint then creating the limit and the smaller moment arm about the MP joint.

Another attribute to notice here is that the -X skew is still present. This implies that the origin of that skewing lies closer to the palm of the hand.

3.2.4 Slightly Larger Object with One Contact Point Near Finger Tip

The configuration that is found in figure 3.12 is very similar to the Natural configuration. We use this as another baseline as we move into some other configurations.

The main differences between this configuration and the Natural configuration (ignoring the fact that one is a clock and the other is a ball), are that this configuration finds the finger more stretched to hold the clock, and the clock is held slightly closer to the palm

The first observation above is probably why the force in the -Y direction is slightly lower than that generated by the Natural configuration. This causes the finger section between the MP joint and the PIP joint to be at a steeper angle than that of the Natural configuration, and that in turn would help reduce the amount of pure downward force (-Y) that can be applied to the object at the contact point. And this is exactly what we see in the graphs.

3.2.5 Two Contact Points on Squared Object

The configuration in figure 3.13 is exactly what we would expect for two opposite contact points. The forces generated at each point are combined with the other to enable the finger to produce large forces in both the + and - X directions.

One interesting characteristic about the XY plot to point out here is the unique pattern that is generated. The configuration gives the finger the ability to produce moderately strong forces in the +X direction. However, the main amount of force can be generated towards (-X,-Y). It is probable that this corresponds to the right side (+X) contact point being attached to the first finger section. That limits the amount of force that can be applied in the -X direction. But if the force is orthogonal to the first finger link (as in the (-X,-Y) direction), then the amount of force that can be applied in that direction is greatly increased.

We can also see the result of the two friction cones on the final outcome as they limit the range of forces that this particular hand configuration can deliver.

3.2.6 Remove One Contact Point from the Squared Object with Two

What happens if we remove the right-most contact point from the above clock example? We generate the graphs found in figure 3.14. The most obvious attribute to notice with these plots is the fact that the -X skewing is gone and only +X forces are present. This makes perfect sense because the vector from the contact point to the Center of Mass is nearly at a 45 degree angle from the vertical. When this vector combines with the friction pyramid (see fig. 2.8), there is nearly no room for -X values. Indeed, this intuition is displayed in the XY force plot for this configuration.

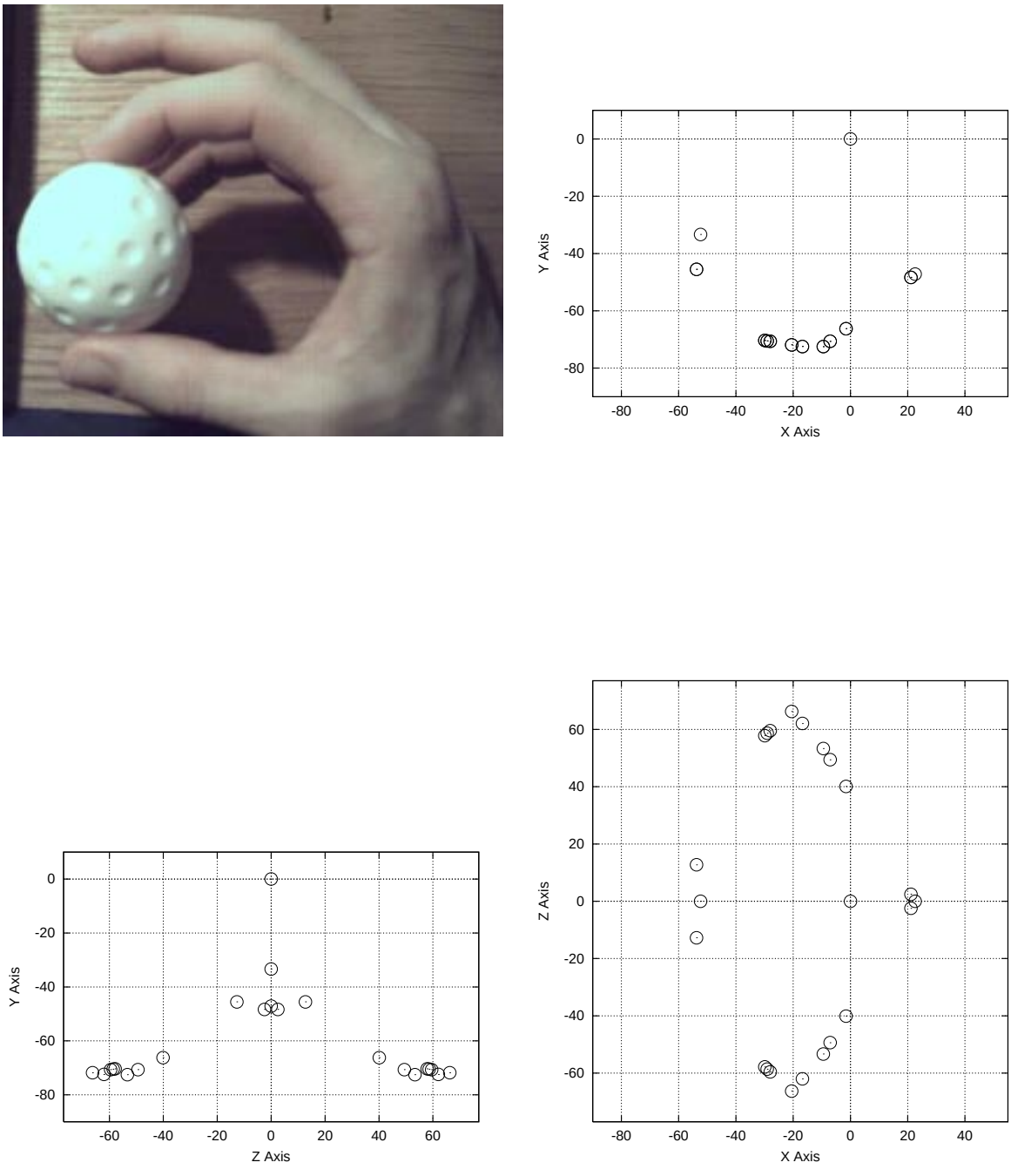

Figure 3.9: Forces for finger in "Natural" Grasping Position.

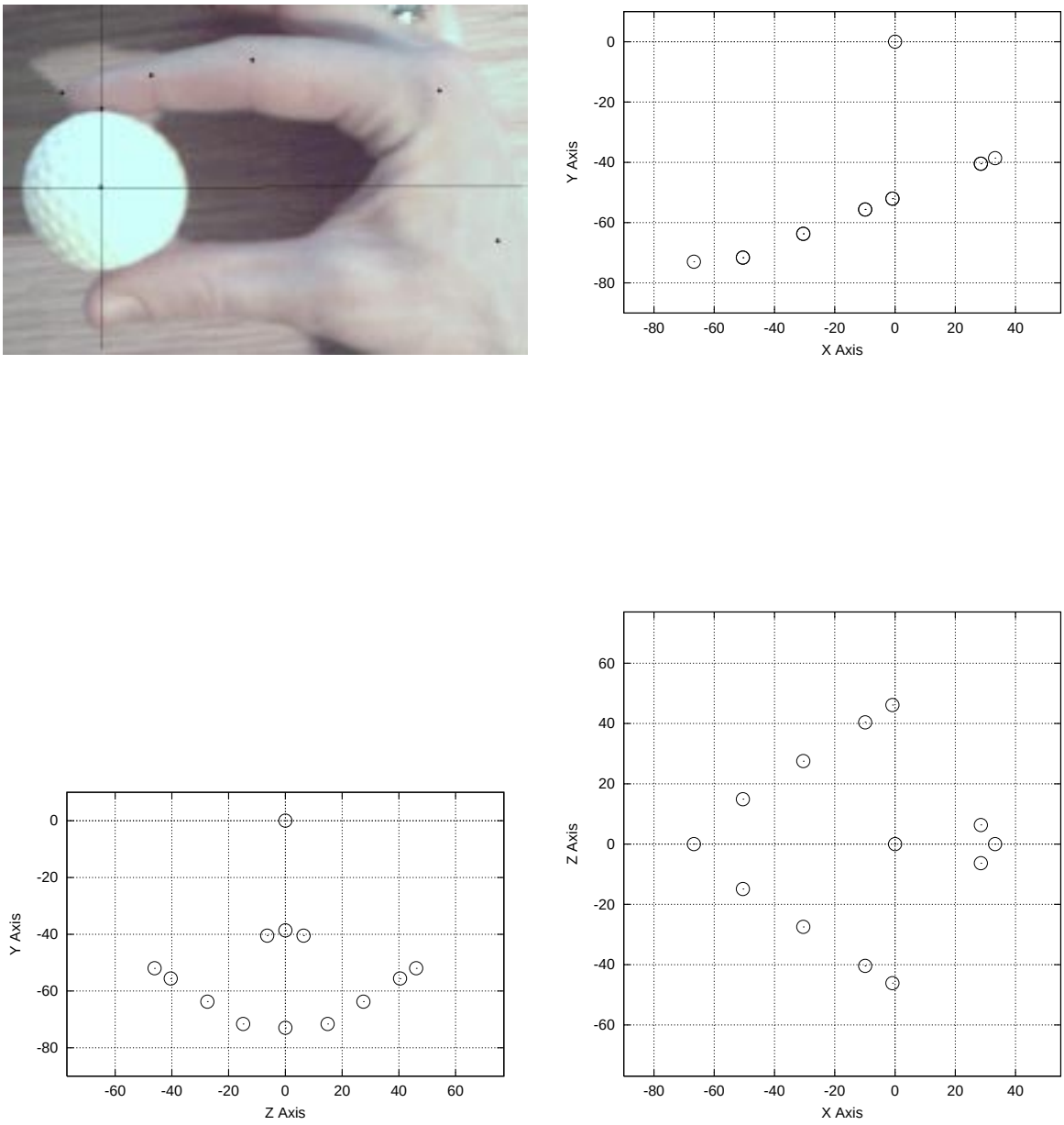

Figure 3.10: An outstretched finger with a single contact point on the third finger pad.

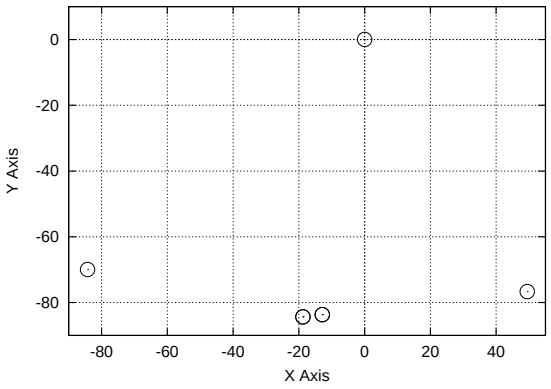

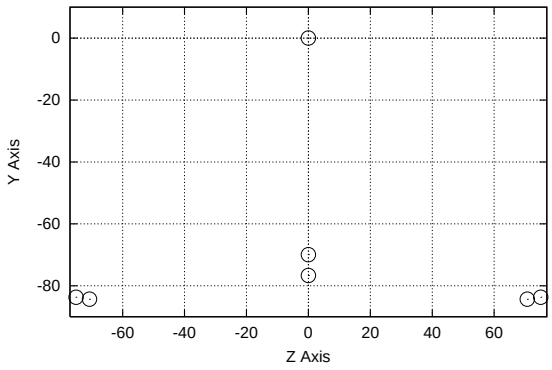

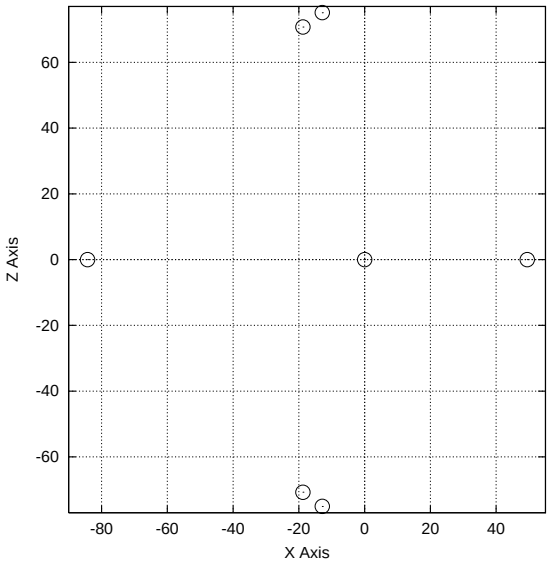

Figure 3.11: An outstretched finger with a single contact point on the second finger pad.

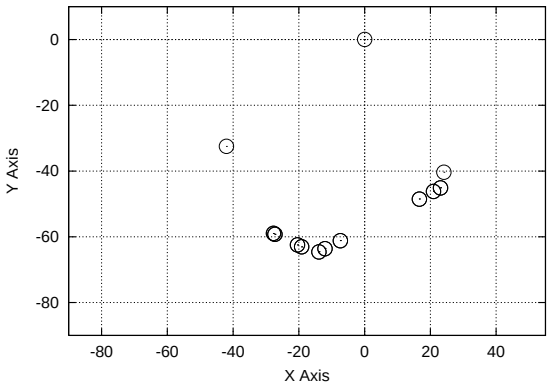

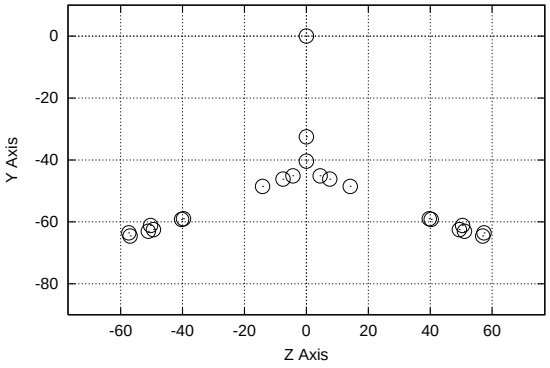

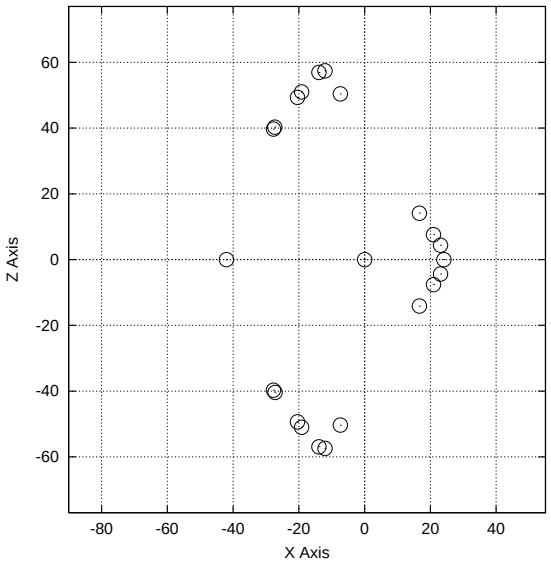

Figure 3.12: This is a finger configuration where the finger has one point of contact on the clock.

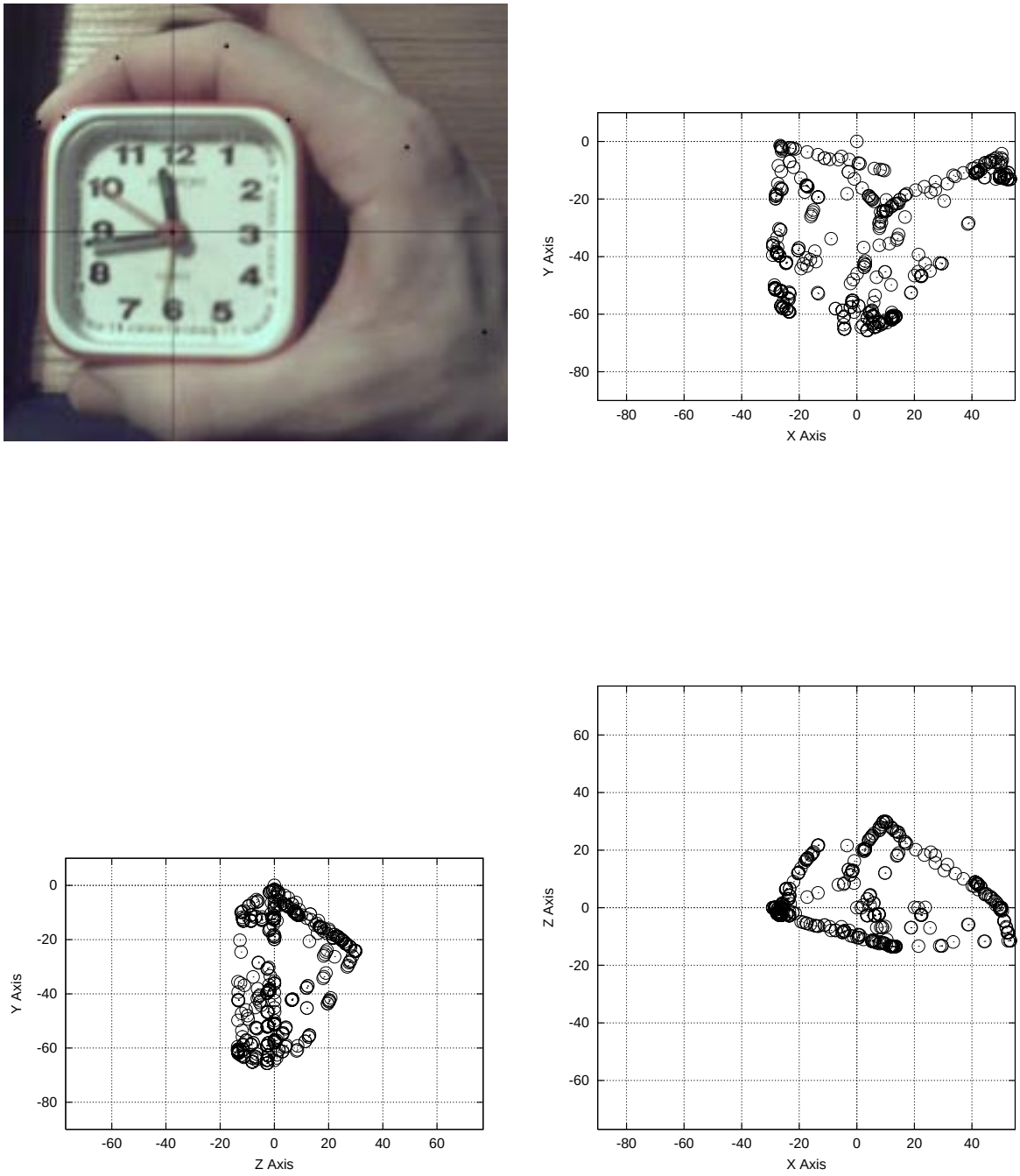

Figure 3.13: A clock being held with two contact points, one at each of the top corners.

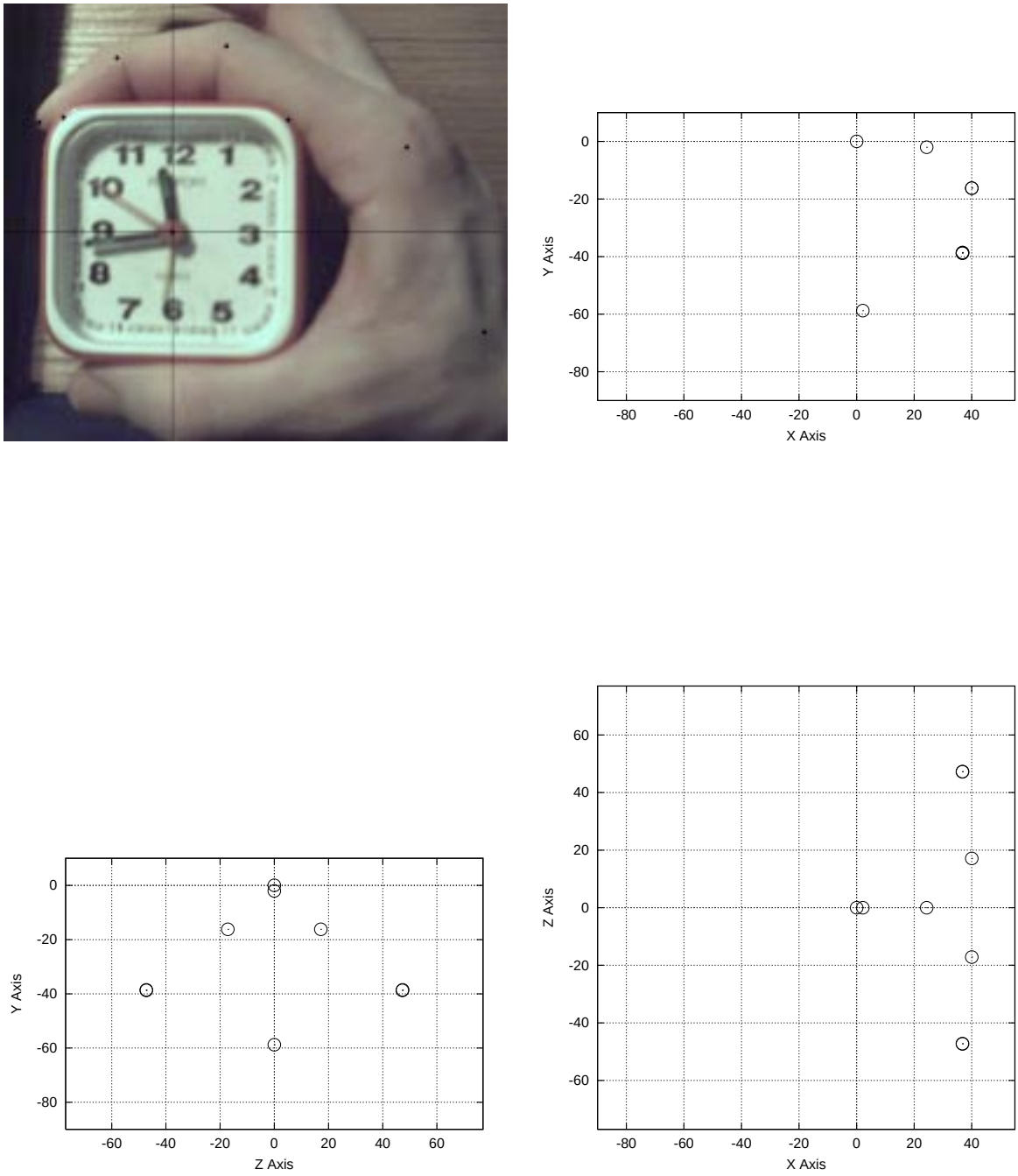

Figure 3.14: The same clock as before, except now we ignore the effects of the right-hand contact point.

Chapter 4

Conclusions

This paper describes a tendon-based finger model for the eventual goal of developing an automated grasp quality measure, and eventually automated animated grasping of objects. This is a small step in that direction.

We have seen that the model described in this paper duplicates the results of human experiments where the muscles of the finger are isolated [**?**]. The results returned from our finger model were about twice that of those observed in human experiments. This is to be expected as we were working out the maximal possible forces that could be generated. It is possible that the difference in our maximal possible forces and those of the human trials is the result of humans not being able to generate true maximum force on queue. It is also possible that people might apply forces with some safety margin automatically built in. More study is needed to find the true answer.

We then looked at how this model might tell us something about different grasps. It certainly produces a wide variety of graphs of possible forces to be applied to an object. We also observed that the force graphs produced varied according to contact point number and location. We believe that it predicts the results of changes in contact point positioning to the extent that the forces clearly move away from the contact point towards the center of mass of the object. This is exactly what should be expected.

As mentioned throughout the paper, this research is the first step in ultimately producing an automated grasping mechanism for animated characters. The next step in the process will be to expand this finger model to include the entire hand. From that model, researchers should be able to determine quality grasps for particular objects according to the forces desired to be applied to those objects.

Bibliography

[1] K. An, E. Chao, W. Cooney, and R. Linscheid. Normative model of human hand for biomechanical analysis. *Journal of Biomechanics*, 12:775–788, 1979.

[2] N. S. Pollard. Synthesizing grasps from generalized prototypes. In *Proc. IEEE Intl. Conference on Robotics and Automation*, Minneapolis, Minnesota, April 1996.

[3] F. Valero-Cuevas. Predictive modulation of muscle coordination pattern magnitude scales fingertip force magnitude over the voluntary range. *Journal of Neurophysiology*, 83(3):1469–1479, 2000.